Primitive Chain Network Simulations for H-Polymers under Fast Shear

[1*]Yuichi Masubuchi, [2]Giovanni Ianniruberto, and [2]Giuseppe Marrucci

[1] *Department of Materials Physics, Nagoya University, Nagoya 4648603, Japan*

[2]*Dipartimento di Ingegneria Chimica, dei Materiali e della Produzione Industriale, Università degli Studi di Napoli "Federico II", Piazzale Tecchio 80-80125 Napoli, Italy*

*To whom correspondence should be addressed

mas@mp.pse.nagoya-u.ac.jp

ABSTRACT

Branchpoint Withdrawal (BPW) has been recognized as one of the important molecular mechanisms for the description of the dynamics of entangled branched polymers under fast flows. However, the relation to the other known molecular mechanisms has not been fully elucidated yet. In this study we performed primitive chain network (i.e., multi-chain slip-link) Brownian simulations for a melt of a well-characterized monodisperse H-polymer, for which the linear viscoelasticity and shear viscosity growth curves at several shear rates are available in the literature. After confirming the consistency of the simulations with the rheological data, we used the simulations to analyze the molecular motion in detail. The results reveal that molecular tumbling occurs in branched polymers just as in linear ones, and that it is accelerated by BPW. Furthermore, BPW not only mitigates backbone stretch, as expected, but also arm stretch. However, because the transient startup viscosity is anyhow dominated by chain stretch dynamics rather than by molecular tumbling, our results rationalize the fact that pom-pom theories successfully ignore tumbling in shear flows.

KEYWORDS

Viscoelasticity, molecular simulations, start-up shear, shear thinning.

Published in SOFT MATTER, **16**, 2020, 1056-1065

INTRODUCTION

Branchpoint withdrawal (BPW)[1] is one of the established molecular mechanisms for the description of branched polymer dynamics under fast flows. In the tube-theory framework, entangled polymer dynamics is focused on the motion of a test molecule subjected to a tube-shaped constraint, representing the mean field exerted by the surrounding molecules.[2] For the case of branched polymers, the arms are confined in their own tubes that emanate from the main tube of the backbone, and the reptation motion of the backbone is triggered by arm retraction.[3] On top of this thermal, hierarchical relaxation, under fast flows an additional relaxation mechanism takes place: the branchpoint is withdrawn into the backbone tube when the tension in the backbone exceeds the entropic barrier of such improbable conformation.[1] As a consequence, the backbone tension is upper limited, and it is presumably lower than the maximum tension determined by the finite chain extensibility. Such a suppressed extension of the backbone has been observed experimentally.[4] The molecular constitutive equation based on this BPW idea, the so-called pom-pom constitutive equation,[1] has attained great success for the description of branched polymer rheology under elongational flows. Several modified models have been proposed for better predictions, and/or numerical convenience, in macroscopic flow calculations.[5–9]

Even though BPW is such a significant mechanism, there are a few open questions concerning the relation to the other known, important molecular mechanisms. For example, several years ago, we discussed about competition between BPW and convective constraint release (CCR).[10] CCR is a flow-induced increase of the relaxation rate for the reptation motion, due to renewal of topological obstacles associated to the relative convective motion among neighboring molecules.[11] Although CCR has been unanimously considered an important molecular mechanism in the dynamics of entangled linear polymers under fast flows, to our knowledge CCR has never been implemented into the pom-pom models, differently from the thermal constraint release, which is accounted for through the so-called tube dilation.[12] Because CCR certainly contributes to the relaxation of the backbone, the occurrence of BPW could be suppressed by CCR via the reduction of the backbone tension. Hence, in order to observe the rate of occurrence of these events, we performed multi-chain slip-link Brownian simulations for a pom-pom polymer melt under fast uniaxial elongation, and showed that for such flows BPW overwhelms CCR.[10] This observation rationalizes absence of CCR in the pom-pom models in elongational flows.

In this study, we examine the contribution of BPW under fast shear flows, also in relation to the shear-induced molecular tumbling motion. In the original pom-pom paper, Larson and McLeish[1] demonstrated that BPW does not play any significant role in shear flows, given that the magnitude of the backbone stretch does not exceed the critical value to overcome the entropic barrier. However, BPW would be activated by the local force balance around the branchpoint even if the entire backbone stretch is not significant. Besides, in shear flows BPW could be affected by the tumbling motion of

the molecules. Recent molecular simulations have shown that polymers undergo a quasi-periodic tumbling motion under shear.[13–15] Although, conceptually, such a flow-induced molecular motion should be included in CCR, Costanzo et al.[16] considered the tumbling motion separately from CCR to explain the stress undershoot at high shear rates. Intuitively, the tumbling motion is expected to occur for branched polymers as well. However, for tumbling to be possible, the network formed among the backbones must be periodically renewed, and BPW is expected to contribute to such a network renewal.

We here report on multi-chain slip-link simulations (so-called primitive chain network simulations[17]) for a well-characterized monodisperse H-polymer melt, for which the linear viscoelasticity[18] and the stress growth at high shear rates[19] are available in the literature. As previously examined for the other branched polymers,[10,20–24] the present simulation semi-quantitatively reproduces the linear viscoelasticity. In view of such agreement, we determined the units of time and stress, and we run the simulations under shear with and without BPW. The simulations with BPW reasonably reproduce the experimental data, whereas those without BPW somewhat overestimate the stress. We next analyzed the molecular motion in detail to conclude that BPW helps the tumbling motion of the backbone, in addition to the expected reduction of stretch. Details are reported below.

MODEL AND SIMULATIONS

Multi-chain slip-link simulations were performed with the extension of the model that includes the topology change around the branchpoint for the hierarchical relaxation[21,22] and BPW.[10] As the simulation scheme used here has already been described in those papers, only a summary is given below.

In the simulation, entangled branched polymers are replaced by a network whose nodes are either crosslinks (the branchpoints) or slip-links (the entanglements). By assuming that the entanglements are binary, each slip-link connects two chains. Hence, four network strands depart from each slip-link, one (or two at most) of such strands possibly consisting of dangling ends. Of course, each molecule is a well-defined branched path connecting several chain ends. The state variables of the system are the position of dangling ends and of network nodes $\{\mathbf{R}_i\}$, the number of monomers in each network strand or dangling end $\{n_i\}$, the number of strands in each subchain $\{Z_j\}$ (subchains connect either consecutive branchpoints of the backbone or a branchpoint to the chain end of the corresponding arm), and the connectivity matrix of the subchains for each molecule $\{C_k\}$. For $\{\mathbf{R}_i\}$, the dynamics is described by a Langevin-type equation of motion, in which the force balance relates the drag force, the tension force acting in each strand emanating from the node, the osmotic force due to density inhomogeneities, and the random force of thermal motion. The kinetics of $\{n_i\}$ is calculated according to the rate equation that takes account of a force balance like that of the $\{\mathbf{R}_i\}$-dynamics, here applied to consecutive strands of the molecule across a slip-link. $\{Z_j\}$ changes with

time due to the creation or destruction of slip-links at the chain ends. Indeed, when the number of monomers on a dangling end becomes smaller than a threshold value because of the kinetics mentioned above, the associated slip-link is removed, and consequently the two strands of each of the two chains merge into one. Conversely, a new slip-link is created when the number of monomers in the chain end exceeds a maximum value, and the companion of the chain end is a strand chosen randomly from the surroundings. Because no chemical reaction is considered, $\{C_k\}$ is kept unchanged throughout the simulations.

The dynamics so far described is enough for linear polymers. For branched ones, additional rules governing topological changes around the branchpoints are necessary. One of such rules is the hierarchical relaxation, according to which reptation of the backbone is allowed when the branching arms relax.[3] In our implementation, we allow the branchpoint to hop across the next slip-link when no slip-link happen to exist on the branching arms emanating from the branchpoint.[21] Following the previous study,[10] we refer to this topological change as branchpoint reptation (BPR). A different possibility is the previously mentioned BPW, when we "suck" the branchpoint and the arms into the slip-link next to the branchpoint when the local tension force in the backbone strand emanating from the branchpoint exceeds the sum of the tension forces of the arm strands.[10]

Although finite chain extensibility and stretch/orientation-induced reduction of friction play some role in elongational flows as reported earlier,[25,26] they are not considered in this study because we focus on the behavior under shear, where they are expected to be only marginally relevant.

In this study, the simulations were performed for a melt of monodisperse H-shaped polystyrene molecules, known by the code H3A1A.[18] The molar mass of the arm and of the backbone are M_a =132k and M_b =123k, respectively. According to the conversion factor for the molar mass for polystyrene melts earlier determined as $M_0 = 11$k,[27,28] the average number of the network strands under equilibrium for the arm and the backbone are $Z_{a0} = 12$, and $Z_{b0} = 11$, respectively.

The units of length, energy, and time used in the simulations are, respectively, the equilibrium strand root-mean-square length a, the thermal energy $k_\mathrm{B}T$, and the diffusion time of the strand $\tau_0 \equiv \zeta a^2/6k_\mathrm{B}T$, where ζ is the friction coefficient of a chain segment with molar mass M_0. The simulations were performed with a periodic boundary condition, for which the box volume was fixed at 10^3. Twelve independent quiescent simulations starting from different initial configurations were run for a sufficiently long period of time, which is more than ten times longer than the longest relaxation time of the system. For the recorded stress fluctuating with time, we disregarded the former half to eliminate possible artifacts arising from the initial state. The linear relaxation modulus was then obtained via the Green-Kubo formula for the remaining latter half. The relaxation modulus was then converted to the complex moduli through fitting to a multi-mode Maxwell function with the help of the REPTATE code.[29] To the equilibrium configurations, as attained in the quiescent simulations, shear flows were applied via a SLLOD-like method, in which a small affine deformation was introduced at

each integration time step. The Lees-Edwards boundary conditions were also employed.

RESULTS

Figure 1 shows linear viscoelasticity simulation results, compared to the experimental data.[18] With the conversion factors for time and modulus that are determined as $\tau_0 = 0.01$s and $G_0 = 0.3$MPa, the simulation (red curves) reasonably reproduces the experimental results (symbols). To be fair, we note that around the crossover of the G' and G'' curves the simulation slightly overestimates the modulus. Because this tendency was also observed for the other H-polystyrenes earlier examined,[24] the discrepancy reasonably implies some (minor) flaw in the model. Not knowing better, we accepted the predicted linear viscoelastic response given in Fig. 1 (with the corresponding equilibrium configurations), and we proceeded with the simulations of shear startup from such initial states.

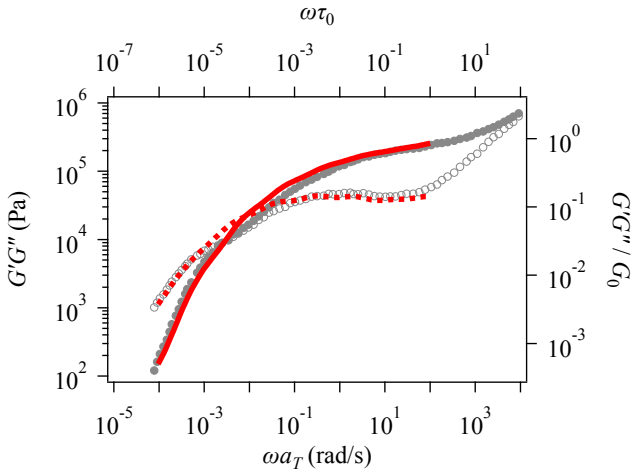

Figure 1 Linear viscoelasticity of H polystyrene melt. Red curves are simulation results, and filled and unfilled circles indicate experimental data[18] at 169.5°C. Solid curve and filled symbols are G', and dotted curve and unfilled symbols are G''.

Figure 2 shows the viscosity growth under fast shear calculated with the time and modulus conversion factors mentioned above. The simulation results are in good agreement with the experimental data[19] if the shear rate is relatively low. As the shear rate increases, the simulation deviates from the data. Specifically, for the viscosity overshoot, the peak appears somewhat later, and the viscosity grows higher. The discrepancy in the viscosity overshoot might be related to the inconsistency in the linear viscoelasticity. Nevertheless, the steady-state viscosity is semi-quantitatively reproduced. Although these features are present both with and without BPW, the simulation with BPW (red curves) better captures the experiment than that without BPW (blue curves). In particular, the simulation without BPW shows a delayed mitigation of the viscosity after the overshoot, *i.e.*, moving towards the steady state. McLeish et al.[30] mentioned that, in the pom-pom

constitutive equation, BPW affects the magnitude of the overshoot, but we do not observe such an effect.

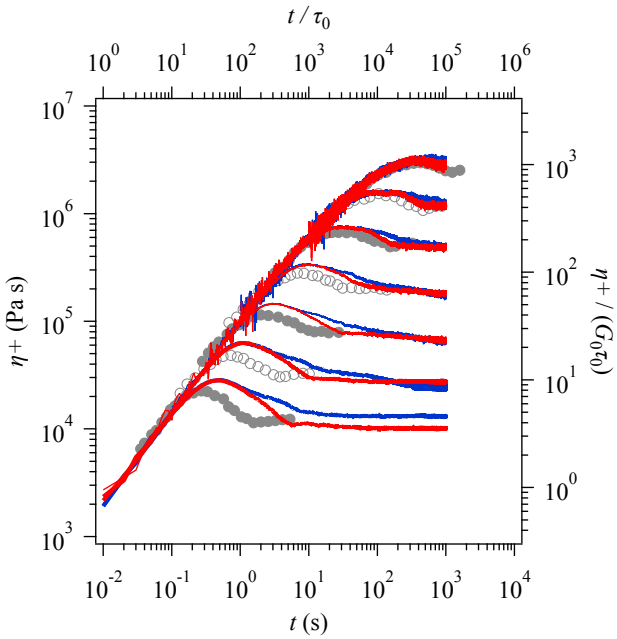

Figure 2 Viscosity growth of H polystyrene melt under fast shear. Shear rate are 0.01, 0.032, 0.1, 0.32, 1, 3.2, and 10 s^{-1}, from top to bottom. Red and blue curves are simulation results with and without BPW, respectively, and both filled or unfilled circles indicate experimental data[19] at 169.5℃.

To see the role of BPW in detail, we analyzed stress, strand stretch, and strand orientation for the arm and backbone subchains separately. Results are shown in Fig. 3 for the case of a shear rate of 10 s^{-1}. As seen in the top panel (as well as in Fig. 2), BPW accelerates relaxation of the stress after the maximum. The decomposed stress shown in the second panel of Fig. 3 reveals that such acceleration comes from the backbone contribution (solid curves). Indeed, in the simulation without BPW (blue curves), relaxation of the backbone stress is delayed. For the arms (broken curves), the transient stress is virtually insensitive to BPW. Moreover, BPW also lowers the steady-state value. These effects of BPW appear to be due to reduction of the strand stretch (third panel). BPW contributes to relief of the stretch for both backbone and arms, and it also lowers the steady state values. Reduction of the backbone stretch is in harmony with the original idea of BPW, whereas reduction of the arm stretch goes beyond the classical tube modeling. The difference in the arm stretch with and without BPW reflects the renewal rate of the entanglement network. As discussed later, BPW accelerates molecular tumbling, which goes together with a renewal of the entanglement network surrounding the tumbling chain. Because the entanglements between backbones and arms are included in such a renewed network, BPW mitigates arm stretch as well as the backbone stretch. The segment orientation

(bottom panel) is not strongly affected by BPW, apart from a weak over-orientation seen in the backbone subchain (blue solid curve). The backbone strand orientation shows a clear undershoot that reflects a rotating motion of the backbone, as shown later.

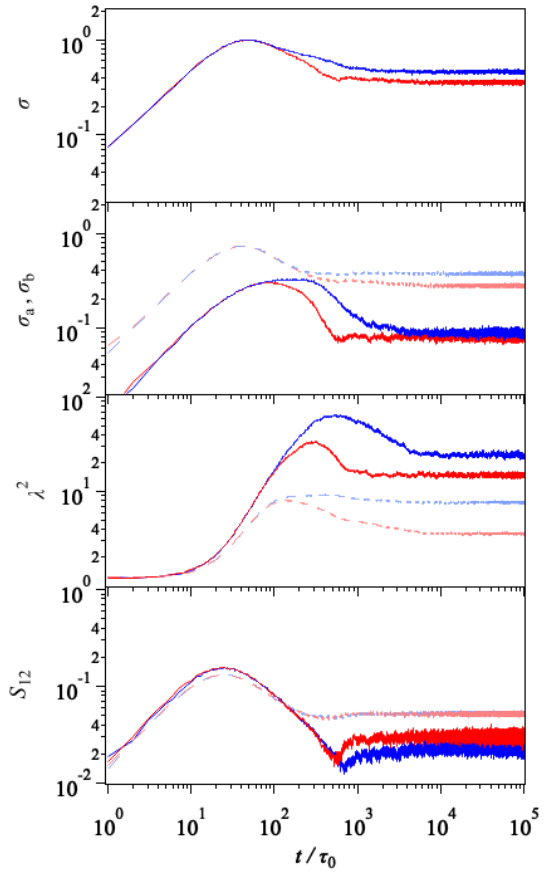

Figure 3 Stress during shear startup for the entire system (top panel), contribution to stress from arms and backbones (2nd panel), squared strand stretch (3rd panel), and strand orientation (bottom panel) at $\dot{\gamma}$ =10 s^{-1}. Red and blue curves are from the simulations with and without BPW, respectively. Solid and dotted curves indicate results for backbones and arms, respectively.

Figure 4 (top panel) shows the rate of BPW and BPR events per molecule, k_{BPW} and k_{BPR}, at the shear rate of 10 s^{-1}. k_{BPW} (green curve) steeply grows in a short time, during which the local tension becomes sufficiently strong due to the deformation. As a result of BPW, the number of entanglements in the backbone decreases with time (as shown by the red curve in the bottom panel), which in its turn makes k_{BPW} to go through an overshoot. Because the peak position of k_{BPW} coincides with that for the strand stretch (see 3rd panel in Fig. 3), we may conclude that relief of the stretch is indeed induced by BPW. k_{BPR} is shown in Fig. 4 by red and black curves for the simulations with and without BPW. k_{BPR} is affected by the convection because the entanglements formed between arms and between arm and backbone are removed by the translational motion of the

molecules, i.e., by CCR. However, even with such a flow-induced enhancement, k_{BPR} is not comparable to k_{BPW} at this specific shear rate. This result means that BPW is the dominating mechanism for the disentanglement of the network of backbones, and it confirms the fact that in pom-pom theories CCR can be ignored. The rate k_{BPR} comes out smaller in the simulation with BPW (red curve) than that without BPW (black curve) because BPW dominates in removing entanglements.

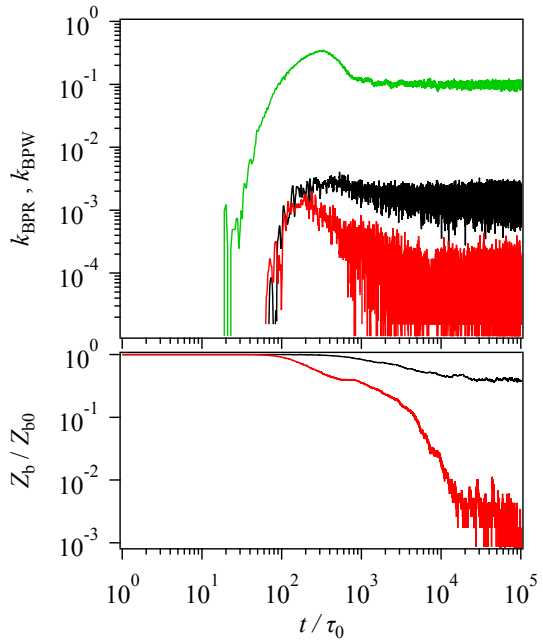

Figure 4 (Top) Time development of the rate of BPW and BPR events per molecule at $\dot{\gamma}$ =10 s^{-1}. For the simulation with BPW, the rate of BPW and BPR is shown by green and red curves. For the simulation without BPW, the BPR rate is shown by the black curve. (Bottom) Number of backbone entanglements (normalized to its equilibrium value) as a function of time. Red and black curves show the results of simulations with and without BPW, respectively.

The bottom panel in Fig. 4 shows the time development of the number Z_{b} of backbone entanglements at $\dot{\gamma}$ =10 s^{-1}, normalized to its equilibrium value Z_{b0}. In the simulation with BPW (red curve) the backbone entanglements are efficiently removed, and their number virtually goes down to zero. Decrease of the backbone entanglements reflects the growth of the BPW rate shown in the top panel. In the simulation without BPW there remain some of the backbone entanglements, which are enough to form a network. This network induces a larger strand stretch, as shown in Fig. 3.

To evaluate the effect of BPW on the rotation of the molecules, we define the rotation angle θ of the backbone in the following way. The pseudo-vector connecting the branchpoints of the H-polymer is projected onto the plane formed by the shear and gradient directions. We then call θ the angle formed by such projection with the shear direction (see top panel in Fig. 5). Although θ is

232 defined in the whole range $]-\pi, \pi]$, at the flow startup ($t = 0$) this angle may be restricted to the
233 range $-\pi/2 < \theta \leq \pi/2$ so that $\cos\theta \geq 0$. The second panel in Fig. 5 shows an example of the
234 time development of $\cos\theta$ at $\dot{\gamma}$ =10 s^{-1}. As reported for linear polymers,[31] $\cos\theta$ exhibits a sort of
235 flip-flop behavior that reflects the molecule rotation under shear. Figure 5 (third panel) is the ensemble
236 average of $\cos\theta\,(t)$ obtained from 100 chains. Because of the random orientations at the initial
237 condition (i.e. all θ values are equally probable), $\langle\cos\theta\,(t = 0)\rangle = 2/\pi$. Next, because of flow,
238 $\langle\cos\theta(t)\rangle$ decays to zero. However, around $t/\tau_0 \sim 1000$, a negative undershoot is found, which
239 clearly indicates a coherent rotation of the different backbones. This feature is also seen in the
240 backbone orientation (going back to the bottom panel of Fig. 3). We further note that the undershoot
241 occurs slightly earlier in the simulation with BPW than in that without BPW. Finally, the bottom panel
242 of Fig. 5 shows the auto-correlation function of $\cos\theta\,(t)$ in the steady state. Here, oscillations around
243 zero start at a time roughly corresponding to that of the undershoot in $\langle\cos\theta(t)\rangle$, although they do
244 not imply coherence among the molecules. We can also infer that BPW augments rotation of the
245 molecule (red vs. blue curve), and the faster rotation causes a more rapid relaxation of the stress after
246 the overshoot via relief of the stretch.
247

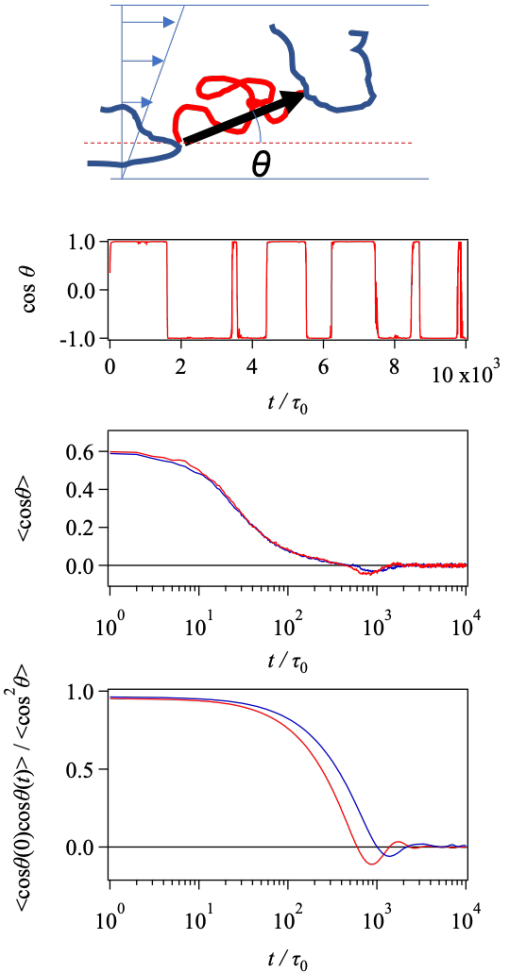

Figure 5 Schematic representation of the rotation angle θ of the backbone (top). Typical example of the time development of $\cos\theta$ after the flow startup at $\dot{\gamma} = 10\ \mathrm{s}^{-1}$ (second top). Ensemble average of $\cos\theta$ (second bottom). Autocorrelation function of $\cos\theta$ in the steady state (bottom). Red and blue curves are the results from the simulations with and without BPW, respectively.

Figure 6 shows the effect of the shear rate on the autocorrelation function of $\cos\theta\,(t)$. The characteristic time for the decay decreases with increasing the shear rate, and the dumped-oscillatory behavior is observed only at high shear rates. These basic features, which are consistent with the earlier report for MD simulations of linear polymers,[14] can be seen for both simulations, with and without BPW.

The Weissenberg number to induce tumbling comes out much higher for the branched polymer here examined than for the linear polyethylene of Nafar-Sefiddashti et al.[14] Indeed, the critical Weissenberg number (beyond which tumbling occurs) reported by them is around 100, whereas it is more than 1000 in this study. This suggests that the branched structure tends to suppress tumbling. Concerning the effect of BPW, it accelerates the decay of correlation, and it induces the dumped-

oscillatory behavior at a shear rate smaller than that for the case without BPW. These observations clearly demonstrate that BPW significantly affects molecular tumbling.

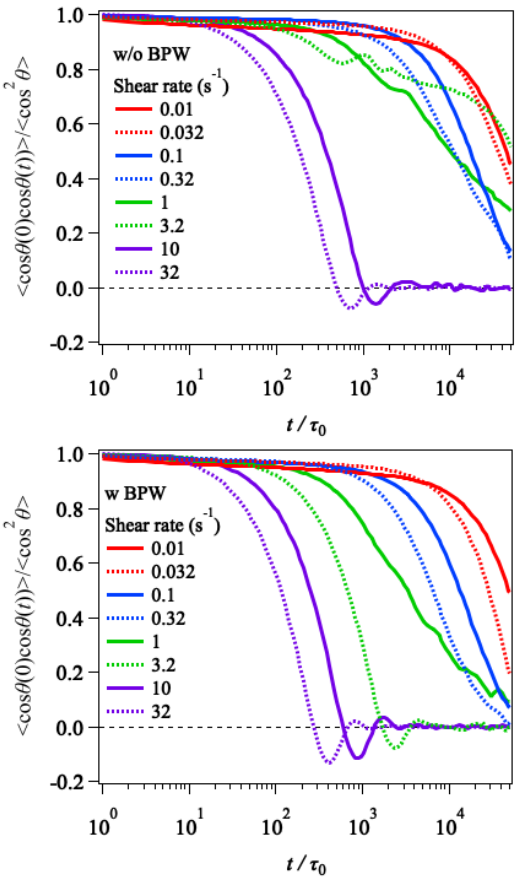

Figure 6 Autocorrelation of $\cos\theta\,(t)$ at several shear rates, with and without BPW (bottom and top panels, respectively).

DISCUSSION AND CONCLUSIONS

Costanzo et al[16] proposed a constitutive equation that accounts for the effect of tumbling under shear to reproduce the stress undershoot following the overshoot. Specifically, they introduced dumped oscillations to the chain strand orientation assuming that tumbling coherence initiated by shear vanishes with time. This idea is consistent with our results shown in Figs 3 and 5, in which we observe some coherence in the rotation of the backbone. Rotation of the backbone also appears as a dumped oscillation in the autocorrelation function of the backbone orientation. However, no stress undershoot is observed because of the contribution of stretch. Indeed, the two bottom panels in Fig. 3 show that the stretch overshoot occurs later than that of the orientation. Consequently, the undershoot of orientation overlaps with the overshoot of stretch, thus cancelling a possible stress undershoot. Besides,

for the H-polymer here examined the total stress is dominated by the contribution of the arms, for which the undershoot of the segment orientation is faint. According to these results, we may conclude that the theory proposed by Costanzo et al[16] does not apply to the H-polymer here examined, and would perhaps be applicable to branched polymers with a different structure.

In conclusion, we investigated the effect of BPW on the motion of branched polymers undergoing fast shear flows using primitive-chain-network simulations for a polystyrene melt of H molecules. The simulation reasonably reproduces the linear viscoelasticity and the shear viscosity growth curve reported in the literature. Based on this agreement with the rheological data, we analyzed the molecular motion in detail. The results demonstrate that BPW reduces the backbone stretch as expected, while it also contributes (unexpectedly) to mitigate the arm stretch. Due to reduction in the stretch, BPW yields better prediction for the viscosity growth under fast shear. Furthermore, BPW accelerates molecular tumbling at high shear rates, although tumbling effects do not explicitly appear in the viscosity growth curve (no undershoot). The rate of BPW is significantly larger than the rate of convection-induced disentanglement. Consequently, it so appears that the reduced chain stretch induced by BPW overwhelms the other stress-determining molecular mechanisms in shear startup. The dominance of BPW is in harmony with our earlier study on a pom-pom polystyrene melt under uniaxial extension, and it also supports pom-pom theories, in which CCR and molecular tumbling are not considered.

ACKNOWLEDGEMENT

This study is supported in part by Grant-in-Aid for Scientific Research (A) (17H01152) and for Scientific Research on Innovative Areas (18H04483) from JSPS.

REFERENCES

1 T. C. B. McLeish and R. G. Larson, *J. Rheol. (N. Y. N. Y).*, 1998, **42**, 81.

2 M. Doi and S. F. Edwards, *The Theory of Polymer Dynamics*, Clarendon press, Oxford, 1986.

3 T. C. B. McLeish, *Europhys. Lett.*, 1988, **6**, 511–516.

4 N. Ruocco, D. Auhl, C. Bailly, P. Lindner, W. Pyckhout-Hintzen, A. Wischnewski, L. G. Leal, N. Hadjichristidis and D. Richter, *Macromolecules*, 2016, **49**, 4330–4339.

5 D. Bick and T. McLeish, *Phys. Rev. Lett.*, 1996, **76**, 2587–2590.

6 N. J. Inkson, T. G. B. McLeish, O. G. Harlen and D. J. Groves, *J. Rheol. (N. Y. N. Y).*, 1999, **43**, 873–896.

7 R. J. Blackwell, O. G. Harlen and T. C. B. McLeish, *Macromolecules*, 2001, **34**, 2579–2596.

8 W. M. H. Verbeeten, G. W. M. Peters and F. P. T. Baaijens, *J. Rheol. (N. Y. N. Y).*, 2001, **45**, 823–843.

9 M. Wagner and V. Rolón-Garrido, *J. Rheol. (N. Y. N. Y).*, 2008, **52**, 1049.

10 Y. Masubuchi, Y. Matsumiya, H. Watanabe, G. Marrucci and G. Ianniruberto, *Macromolecules*, 2014, **47**, 3511–3519.
11 G. Marrucci, *J. Nonnewton. Fluid Mech.*, 1996, **62**, 279–289.
12 G. Marrucci, *J. Polym. Sci. Polym. Phys. Ed.*, 1985, **23**, 159–177.
13 M. H. Nafar Sefiddashti, B. J. Edwards and B. Khomami, *J. Rheol. (N. Y. N. Y).*, 2016, **60**, 1227–1244.
14 M. H. Nafar Sefiddashti, B. J. Edwards and B. Khomami, *J. Rheol. (N. Y. N. Y).*, 2015, **59**, 119–153.
15 M. H. Nafar Sefiddashti, B. J. Edwards and B. Khomami, *Phys. Rev. Fluids*, 2017, **2**, 083301.
16 S. Costanzo, Q. Huang, G. Ianniruberto, G. Marrucci, O. Hassager and D. Vlassopoulos, *Macromolecules*, 2016, **49**, 3925–3935.
17 Y. Masubuchi, J.-I. Takimoto, K. Koyama, G. Ianniruberto, G. Marrucci and F. Greco, *J. Chem. Phys.*, 2001, **115**, 4387.
18 J. Roovers, *Macromolecules*, 1984, **17**, 1196–1200.
19 F. Snijkers and D. Vlassopoulos, *Rheol. Acta*, 2014, **53**, 935–946.
20 Y. Masubuchi, G. Ianniruberto, F. Greco and G. Marrucci, *Model. Simul. Mater. Sci. Eng.*, 2004, **12**, S91–S100.
21 Y. Masubuchi, G. Ianniruberto, F. Greco and G. Marrucci, *Rheol. Acta*, 2006, **46**, 297–303.
22 Y. Masubuchi, T. Yaoita, Y. Matsumiya and H. Watanabe, *J. Chem. Phys.*, 2011, **134**, 194905.
23 Y. Masubuchi, Y. Matsumiya, H. Watanabe, S. Shiromoto, M. Tsutsubuchi and Y. Togawa, *Rheol. Acta*, 2012, **51**, 1–8.
24 Y. Masubuchi, A. Pandey, Y. Amamoto and T. Uneyama, *J. Chem. Phys.*, 2017, **147**, 184903.
25 T. Yaoita, T. Isaki, Y. Masubuchi, H. Watanabe, G. Ianniruberto and G. Marrucci, *Macromolecules*, 2011, **44**, 9675–9682.
26 T. Yaoita, T. Isaki, Y. Masubuchi, H. Watanabe, G. Ianniruberto and G. Marrucci, *Macromolecules*, 2012, **45**, 2773–2782.
27 Y. Masubuchi, G. Ianniruberto, F. Greco and G. Marrucci, *J. Nonnewton. Fluid Mech.*, 2008, **149**, 87–92.
28 Y. Masubuchi and T. Uneyama, *Soft Matter*, 2018, **14**, 5986–5994.
29 A. Likhtman and J. Ramirez, REPTATE.
30 T. Mcleish, J. Allgaier, D. Bick, G. Bishko, P. Biswas, R. Blackwell, B. Blottière, N. Clarke, B. Gibbs, D. Groves, A. Hakiki, R. Heenan, J. Johnson, R. Kant, D. Read and R. Young, *Macromolecules*, 1999, **32**, 6734–6758.
31 Y. Masubuchi, G. Ianniruberto and G. Marrucci, *Nihon Reoroji Gakkaishi*, 2018, **46**, 23–28.